Proceedings of the 29th Annual International
Conference of the IEEE EMBS
Cité Internationale, Lyon, France
August 23-26, 2007.

Modeling of Needle Steering via Duty-Cycled Spinning

Davneet S. Minhas, Johnathan A. Engh, Michele M. Fenske, Cameron N. Riviere, *Member, IEEE*

***Abstract*—As flexible bevel tip needles are inserted into tissue, a deflection force causes the needle to bend with a curvature dependent on relative stiffness and bevel angle. By constantly spinning the needle during insertion, the bevel angle is essentially negated and a straight trajectory can be achieved. Incorporating duty-cycled spinning during needle insertion provides proportional control of the curvature of the needle trajectory through tissue. This paper proposes a kinematic model for needle steering via duty-cycled spinning. Validation using experimental results is also presented.**

I. Introduction

The percutaneous insertion of needles is perhaps one of the most common practices employed in modern clinical practice. Such procedures range from medical diagnosis to therapeutic agent delivery. However, physicians and surgeons often rely only on kinesthetic feedback from the instrument, with no visual feedback from below the skin's surface. Such practices can result in a mitigation of treatments and diagnoses. Complications can arise in biopsy, in which malignancies may not be accurately diagnosed due to poor positioning of the needle tip [1]; anaesthesia, in which improper needle placement can create traumatic effects [2]; and brachytherapy, in which radioactive seeds may sometimes be placed far from those locations preplanned for optimal dosage [3].

Techniques for needle steering and trajectory planning have become a focus of recent research due to the potential for increasing the accuracy and efficacy of current needle insertion practices [4]-[7]. In addition, needle steering and trajectory planning techniques also have the potential for improving upon procedures not inherently dependent on needle insertion. In the realm of neurosurgery, stereotactic techniques are capable of accurate targeting of deep structures within the brain. However, the development of a system which could travel reliably along non-linear trajectories into the brain would significantly increase the versatility of minimally invasive brain surgery. Such technology could be used to steer around critical structures to reach a target, or to target multiple points within a specific region without significant disturbance of the overlying surface of the brain.

We have previously shown qualitatively that duty-cycled spinning of a flexible bevel tip needle can effectively produce a wide variety of trajectories in tissue [8]. When the flexible bevel tip needle is inserted without spinning, the needle follows a trajectory with some natural curvature dependent on the relative needle stiffness and bevel angle. When the needle is inserted with constant spinning, at a rate relatively larger than the needle insertion velocity, straight trajectories can be achieved. Combining periods of needle spinning with periods of non-spinning, any number of needle curvatures can be achieved, ranging from the natural curvature of the needle to zero curvature.

In this paper, we present a kinematic model quantitatively describing the needle trajectory, based on the duty cycle of spinning and natural curvature of the needle. The model is then validated using experimental results.

II. Methods

A. Needle Steering Model via Duty-Cycled Spinning

A nonholonomic model for bevel-tip needle steering was presented and validated in [4]. Though the work presented did not involve spinning, the model includes a term for rotational speed and therefore is already suited to modeling the spinning behavior. As seen in Fig. 1, this model follows a variation of the standard kinematic bicycle model with constant front wheel angle, φ, wheel to wheel distance, l_1, back wheel to needle tip distance, l_2, insertion speed, u_1, and rotation speed, u_2.

Assuming u_1 and u_2 are control inputs, the kinematic model follows as

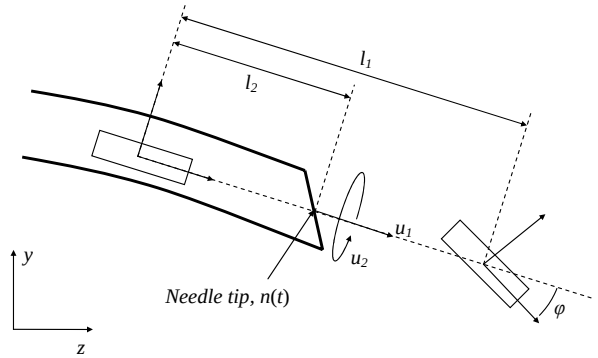

Fig. 1. Configuration of bicycle model parameters during insertion of flexible bevel tip needle (redrawn after [4]).

Manuscript received April 16, 2007. This work was supported in part by the Simeon M. Jones, Jr. and Katharine Reed Jones Fund and the Walter L. Copeland Fund of The Pittsburgh Foundation, and by the National Science Foundation (grant no. EEC-9731748).

D. S. Minhas is with the Biomedical Engineering Department, Carnegie Mellon University, Pittsburgh, PA 15213 (e-mail: dminhas@cmu.edu).

J. A. Engh is with the Department of Neurological Surgery, University of Pittsburgh, Pittsburgh, PA 15213 (e-mail: EnghJA@umpc.edu).

M. M. Fenske is with the Medical Physics Department, Cleveland State University, Cleveland, OH 44115 (e-mail: m.m.fenske@csuohio.edu).

C. N. Riviere is with the Robotics Institute, Carnegie Mellon University, Pittsburgh, PA 15213 (e-mail: camr@ri.cmu.edu).

$$g_{ab}(t) = g_{ab}(0)e^{(u_1\hat{V}_1 + u_2\hat{V}_2)t}$$
$$n(t) = R_{ab}(t)l_2 e_3 + p_{ab}(t), \quad (1)$$

where $R_{ab}(t)$ and $p_{ab}(t)$ are the 3-dimensional rotation and translation components, respectively, of the homogeneous transformation matrix $g_{ab}(t)$, and $n(t)$ represents the needle tip coordinates. Vectors $V_1, V_2 \in \mathbb{R}^6$ are the twist coordinates of the twists $\hat{V}_1, \hat{V}_2 \in se(3)$ [9], such that

$$V_1 = \begin{bmatrix} e_3 \\ \kappa e_1 \end{bmatrix} \text{ and } V_2 = \begin{bmatrix} 0_{3x1} \\ e_3 \end{bmatrix}. \quad (2)$$

e_1, e_2, and e_3 represent *x*-, *y*-, and *z*- coordinate unit vectors respectively, and

$$\kappa = \frac{\tan(\phi)}{l_1} \quad (3)$$

is the curvature of the arc created by the bevel-tipped needle passing through tissue. Further mathematical details of the model are presented in [4].

In order to incorporate a duty cycle of $D = (\tau / T)$ into the kinematic model, where τ is the time of rotation and T is the duty cycle period, we made time dependent adjustments to u_1 and u_2 such that

$$u_1(t) = \sigma$$
$$u_2(t) = \begin{cases} \omega, & jT \le t < T(j+D),\ j = 0,1,2,\ldots \\ 0, & else \end{cases} \quad (4)$$

where $\omega >> \sigma$. Substituting (4) into (1) provides

$$g_{ab}(t) = \begin{cases} g_{ab}(0)e^{(\sigma\hat{V}_1 + \omega\hat{V}_2)t}, & jT \le t < T(j+D),\ j = 0,1,2,\ldots \\ g_{ab}(0)e^{\sigma\hat{V}_1 t}, & else \end{cases}$$
$$n(t) = R_{ab}(t)l_2 e_3 + p_{ab}(t), \quad (5)$$

a kinematic model for duty cycle steering of a bevel tip needle.

B. Experimental Validation

The model was validated using the experimental results from [8]. The needle steering prototype utilized is similar to the telescoping support device presented in [5]. The bevel tip needle is attached to a DC-micromotor in order to control rotational speed. This rotational subassembly is, in turn, attached to a linear slide which is actuated manually, with insertion depth monitored by a magnetic linear displacement sensor.

The needle used for experimentation was a custom built prototype, consisting of a 1.27 mm diameter stainless steel hypodermic needle tip attached to a 0.28 mm diameter nitinol wire. The tip had a 10º bevel and was bent an additional 15º at a distance of 6.3 mm from the end of the tip.

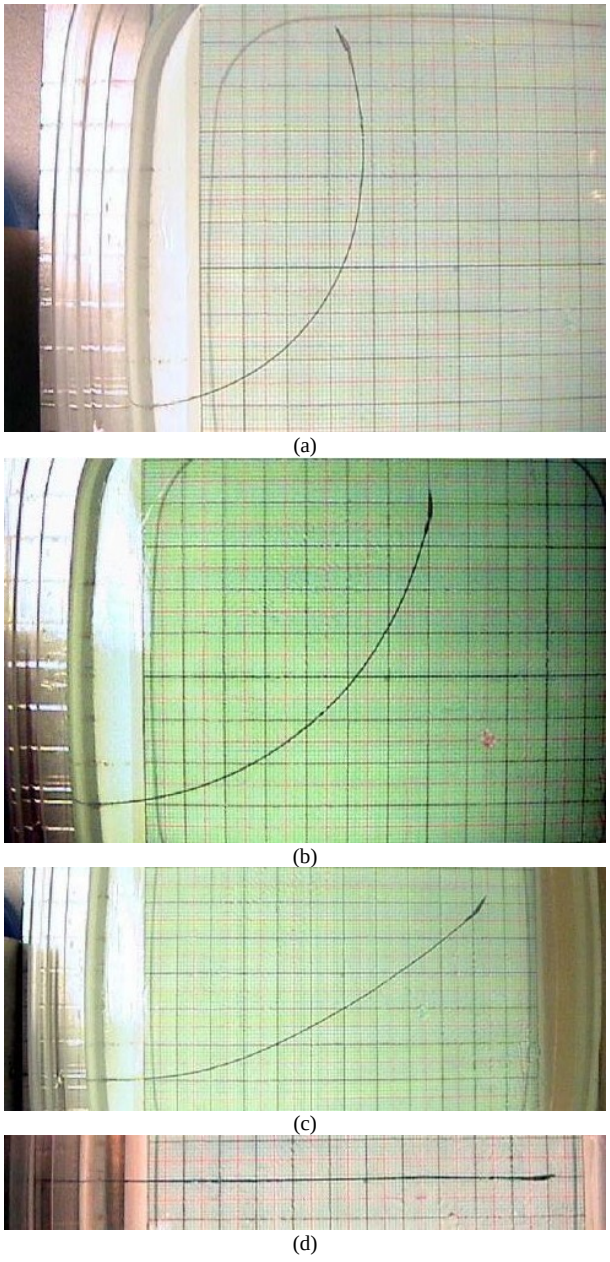

(a) (b) (c) (d)

Fig. 2. Experimentally obtained trajectories of a flexible bevel tip needle at various duty cycles. (a) 0% duty cycle (no spinning). (b) 33% duty cycle. (c) 67% duty cycle. (d) 100% duty cycle (constant spinning).

The *in vitro* test material used during experimentation was Knox gelatin, Kraft Foods Global Inc., mixed at a ratio of 20 cm^3 water to 1.3 cm^3 gelatin. This mixture was used previously as a brain tissue substitute [10] due to it having a similar insertion force profile to that of brain tissue *in vitro*. Gelatin samples were prepared in a number of small, clear bowls corresponding to the number of experimental trials. Each bowl had a small hole cut into the side prior to gelatin

preparation, in order to allow for needle insertion. Such preparation of test media was done in order to ensure uniform mechanical properties for the gelatin across trials, and to avoid inhomogeneities caused by preexisting needle tracks. A mat with a 1 cm square grid was placed beneath the bowls in order to provide a physical reference for digital images taken of the needle trajectories.

For each trial, the needle was inserted with an approximately constant insertion speed, u_1, and a rotation speed, u_2, of 2 rev/sec. Trials for duty cycles of 0%, 33%, 67%, and 100% were performed.

The resulting digital images of the various trials (Fig. 2) were used to extract twenty points in pixel coordinates of each of the needle trajectories. Nine previously designated calibration points in both pixel coordinates and physical coordinates were also obtained. Registration between pixel space and physical space was performed by use of the Iterative Closest Point (ICP) algorithm. This allowed transformation of the needle trajectory from pixel coordinates to physical coordinates. The insertion point coordinates for each needle trajectory was subtracted from the entire trajectory so that each began at the origin in physical space.

A single arc generated by the kinematic bicycle model, (1), beginning at the origin, has a center at

$$c = \begin{bmatrix} 0 \\ -1/\kappa \\ -l_2 \end{bmatrix}, \tag{6}$$

and a radius of

$$r = \sqrt{(l_2)^2 + (\kappa)^{-2}}\,. \tag{7}$$

Note that the sign of κ denotes the direction of the needle trajectory, with a negative κ signifying upward curvature. Utilizing the equation of a circle in the *zy* coordinate system plane,

$$r^2 = (z - e_3{}^T c)^2 + (y - e_2{}^T c)^2\,, \tag{8}$$

in conjunction with the Matlab function *solve*, which finds the zeroes of any given symbolic function, the $\hat{y}$ prediction value is attainable for any given z value. This inverse kinematic model was fit to the experimental data using the Matlab function *nlinfit*, which uses least squares regression to estimate the coefficients of a nonlinear regression function.

Model parameters for each of the needle trajectories through the phantom tissue were derived using the inverse kinematics. The parameters obtained from the experimental 0% duty cycle trajectory were imposed on the forward kinematic model in order to provide a model basis. The 33%, 67%, and 100% duty cycle trajectories, seen in Fig. 3, were then simulated using the 0% trajectory model parameters. The inverse kinematics were again used, in order to derive the 33%, 67%, and 100% duty cycle simulated trajectory model parameters.

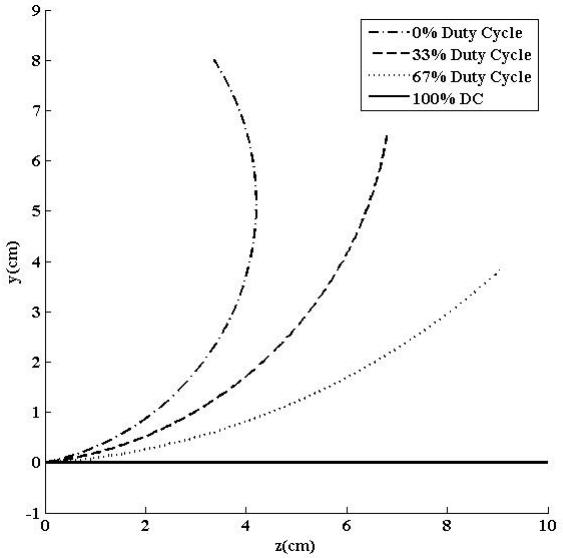

Fig. 3. Simulated trajectories of a flexible bevel tip needle at various duty cycles.

III. Results

The results of the model parameter derivation for the experimental needle trajectories are shown in Table 1. The results of the model parameter derivation for the simulated needle trajectories are shown in Table 2.

TABLE I
EXPERIMENTAL TRAJECTORY MODEL PARAMETERS

Duty Cycle (%)	κ (cm^{-1})	l_2 (cm)	RMS error (cm)
0	-0.1938	1.0633	0.0225
33	-0.1224	0.7033	0.0213
67	-0.0695	1.4162	0.0340
100	-0.0000	1043.2	0.0118

Model parameters (κ, l_2) for experimentally obtained trajectories of 0%, 33%, 67%, and 100% duty cycles, and the RMS error of model fit.

TABLE 2
SIMULATED TRAJECTORY MODEL PARAMETERS

Duty Cycle (%)	κ (cm^{-1})	l_2 (cm)	RMS error (cm)
0	-0.1938	1.0633	0.0000
33	-0.1339	0.9131	0.0100
67	-0.0644	0.7508	0.0072
100	-0.0000	-2.9853	0.0000

Model parameters (κ, l_2) for simulated trajectories of 0%, 33%, 67%, and 100% duty cycles, and the RMS error of model fit.

While the root mean squared error between experimental trajectory and simulated trajectory κ values is 0.0063 cm^{-1}, the deviation between experimental and simulated trajectory l_2 values is much larger. In single curve trajectories such as those presented here, l_2 dictates the z-coordinate of the

center of the arc. Assuming l_2 is zero implies that the needle is entering the tissue at a point where the derivative of the generated arc is equal to zero. Variations in l_2 from zero imply a modification in the initial entry angle of the needle. Conversely, curvature dictates both the arc center y-coordinate and the radius of the trajectory arc, having more of an effect than l_2 on generated single curve needle trajectories as the needle travels through tissue. Essentially, the deviation between experimental and simulated trajectory l_2 values denotes a variability in initial entry angle which could have been cause by slight kinking outside of the tissue or improper alignment of the needle and the gelatin. As a result, the model is still considered to be a good fit due to the very low curvature error. Fig. 4 qualitatively supports the model as a good fit, showing a linear relationship between curvature and duty cycle for both the simulated and experimental needle trajectories.

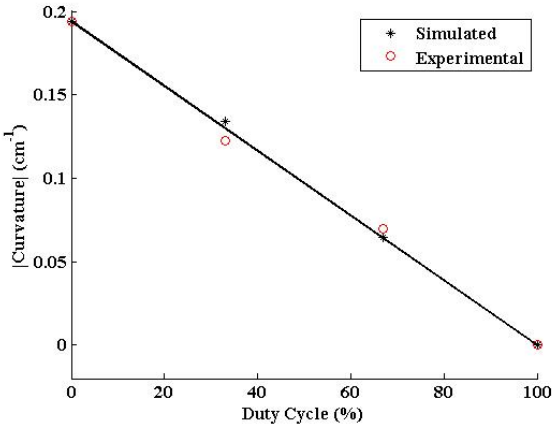

Fig. 4. Needle curvature vs duty cycle relationship for both experimental and simulated trajectories.

IV. DISCUSSION

An accurate kinematic model that quantitatively describes needle steering via duty-cycled spinning allows for a variety of possibilities in surgical procedures. Preoperative trajectory planning [11]-[13] and intraoperative closed-loop systems incorporating duty-cycled spinning become possibilities. Current invasive surgical procedures can be performed minimally invasively, reducing tissue manipulation and exposure. Improvements in current diagnosis and treatment accuracy also become attainable.

Ongoing and future research activities include further validation of the kinematic model for needle insertion via duty-cycled spinning, specifically in three dimensions as opposed to planar insertion. Modeling of needle steering in heterogeneous tissue is an additional further direction, as this would be more representative of steering in the brain. The creation of a closed-loop system incorporating image guidance will also be pursued, and i*n vitro* testing in both human cadaver and animal tissue will follow.

REFERENCES

[1] M. A. Hau, J. I. Kim, S. Kattapuram, F. J. Hornicek, A. E. Rosenberg, M. C. Gebhardt, H. J. Mankin, "Accuracy of CT-guided biopsies in 359 patients with musculoskeletal lesions," *Skeletal Radiology*, vol. 31, no. 6, pp. 349-353, 2002.

[2] T. T. Horlocker, D. J. Wedel, H. Benzon, D. L. Brown, F. K. Enneking, J. A. Heit, M. F. Mulroy, R. W Rosenquist, J. Rowlingson, M. Tryba, C. S. Yuan, "Regional anesthesia in the anticoagulated patient: defining the risks (the second ASRA Consensus Conference on Neuraxial Anesthesia and Anticoagulation)," *Reg. Anesth. Pain Med.*, vol. 28, no. 3, pp. 172-197, May-June 2003.

[3] J. F. Corbett, J. J. Jezioranski, J. Crook, T. Tran, I. W. T. Yeung, "The effect of seed orientation deviations on the quality of ^{125}I prostate implants," *Phys. Med. Bio.*, vol. 46, pp. 2785-2800, 2001.

[4] R. J. Webster III, J. S. Kim, N. K. Cowan, G. S. Chirikjian, A. M. Okamura, "Nonholonomic modeling of needle steering," *Int. J. Rob. Res.*, vol. 25, no. 5-6, pp. 509-525, May-June 2006.

[5] R. J. Webster III, J. Memisevic, A. M. Okamura, "Design considerations for robotic needle steering," in *Proc. IEEE Int. Conf. Rob. Autom.*, 2005, pp. 3599-3605.

[6] S. P. DiMaio, S. E. Salcudean, "Needle insertion modeling and simulation," *IEEE Trans. Rob. Autom.*, vol. 19, no. 5, pp. 864-875, October 2003.

[7] S. Okazawa, R. Ebrahimi, J. Chuang, S. E. Salcudean, R. Rohling, "Hand-held steerable needle device," *IEEE ASME Trans. Mechatron.*, vol. 10, no. 3, June 2005.

[8] J. A. Engh, G. Podnar, D. Kondziolka, C. Riviere, "Toward effective needle steering in brain tissue," in *Proc. 28th Annual Int. Conf. IEEE Eng. Med. Biol. Soc.*, 2006, pp. 559-562.

[9] R. M. Murray, Z. Li, S. S. Sastry, *A Mathematical Introduction to Robotic Manipulation*. Boca Raton: CRC Press, 1994.

[10] R. C. Ritter, E. G. Quate, G. T. Gillies, M. S. Grady, M. A. Howard III, W. M. Broaddus, "Measurement of friction on straight catheters in *in vitro* brain and phantom material," *IEEE Trans. Biomed. Eng*, vol. 45, no. 4, pp. 476-485, April 1998.

[11] R. Alterovitz, K. Goldberg, J. Pouliot, R. Taschereau, I. C. Hsu, "Sensorless planning for medical needle insertion procedures," in *Proc. IEEE Int. Conf. Intell. Rob. Sys.*, 2003, pp. 3337-3343.

[12] R. Alterovitz, K. Goldberg, A. Okamura, "Planning for steerable bevel-tip needle insertion through 2D soft tissue with obstacles," in *Proc. IEEE Intl. Conf. Rob. Autom.*, 2005, pp. 1652-1657.

[13] W. Park, J. S. Kim, Y. Zhou, N. J. Cowan, A. M. Okamura, G. S. Chirikjian, "Diffusion-based motion planning for a nonholonomic flexible model," in *Proc. IEEE Int. Conf. Rob. Autom.*, 2005, pp. 4611-4616.